2022 METAvivor Award Final Report

PI: Lin Zhang, M.D., Ph.D. Research Assistant Professor, Department of Molecular and Cellular Oncology, The University of Texas MD Anderson Cancer Center

Co-PI: Dihua Yu, M.D., Ph.D. Professor and Chair, Department of Molecular and Cellular Oncology, The University of Texas MD Anderson Cancer Center

Grant Title: Altering the Metabolic Tumor Microenvironment to Impede Breast Cancer Brain Metastasis

Date: June 11th, 2025

Project goals: The primary goal of this project is to determine whether and how glutamine blockade impede breast cancer (BC) brain metastasis (BrM) outgrowth.

To achieve the goals outlined above, we proposed the following two Specific Aims. Over the past year, we have made significant progress in support of these aims. In our Year 1 Progress Report, we reported the following: 1) The glutamine antagonist JHU083 and the GLS inhibitor CB839 are capable of crossing the blood-brain barrier and effectively inhibiting GLS function within BrM lesions and surrounding brain tissues. 2) Both JHU083 and CB839 significantly impeded BC BrM outgrowth in the WHIM3.Br patient-derived xenograft (PDX) triple negative BC (TNBC) model without observable toxicity. Notably, JHU083 demonstrated superior efficacy compared to CB839 in suppressing BrM progression in an immunodeficient mouse model. 3) Glutamine blockade altered the levels of other amino acids, suggesting potential cooperative mechanisms between glutamine depletion and the disruption of other metabolic pathways in promoting cancer cell death. In the second year of funding, our work focused on examining the effects of genetic modification of GLS and SLC1A5 on BrM, as well as evaluating the efficacy of JHU083 in inhibiting BrM in an immunocompetent mouse model. We have successfully advanced both Specific Aims and uncovered several unexpected yet insightful discoveries that further strengthen our research.

Aim 1. Determine the contribution of glutamine metabolic dysregulation to BC BrM development. *Specifically, we proposed to examine the impact of* ***(1)*** *loss- and* ***(2)*** *gain-of SLC1A5 and/or GLS functions on BC BrM progression.*

SLC1A5 is the glutamine transporter[1], and GLS is the key enzyme regulating the conversion of glutamine to glutamate[2]. WHIM3 is a PDX TNBC model[3] and Br cells are the brain-seeking sublines developed after 3 rounds of *in vivo* selection in Yu lab. We used the CRISPR-Cas9 system with specific single guide RNAs to knock out SLC1A5 or GLS in WHIM3Br cells. Following selection, single-colony expansion, and confirmation of protein expression, we successfully obtained four GLS knockout clones (sgGLS_2 clones #2, #5, and #6; sgGLS_6 clone #8) that showed complete depletion of GLS expression (Figure 1A). Due to the lower knockout efficiency of SLC1A5, we screened over 100 clones and ultimately identified two single clones (sgSLC1A5_1 clones #1 and #36) with confirmed depletion of SLC1A5 expression (Figure 1A). We combined the four GLS knockout clones to generate a pooled multi-clone mixture (sgGLS), and similarly combined the two SLC1A5 knockout clones to create a two-clone mixture (sgSLC1A5). A control mixture (sgCtrl) was also prepared from non-targeting control clones. To assess the impact of GLS or SLC1A5 loss on BrM progression, we injected 100,000 WHIM3Br.sgCtrl, WHIM3Br.sgGLS, or WHIM3Br.sgSLC1A5 cells into the carotid artery (ICA) of nude mice. BrM development was monitored via in vivo bioluminescence imaging (BLI) and fluorescence imaging. Mice injected with WHIM3Br.sgCtrl cells developed BrM significantly faster than those injected with WHIM3Br.sgGLS cells, while BrM formation was rarely observed in mice injected with WHIM3Br.sgSLC1A5 cells (Figure 1B–1E). Furthermore, mice receiving WHIM3Br.sgCtrl cells had significantly shorter BrM-free survival compared to those injected with WHIM3Br.sgSLC1A5 cells (Figure 1F). These in vivo results clearly demonstrate that depletion of GLS or SLC1A5 delays BrM progression, highlighting the essential role of glutamine metabolism in BrM development.

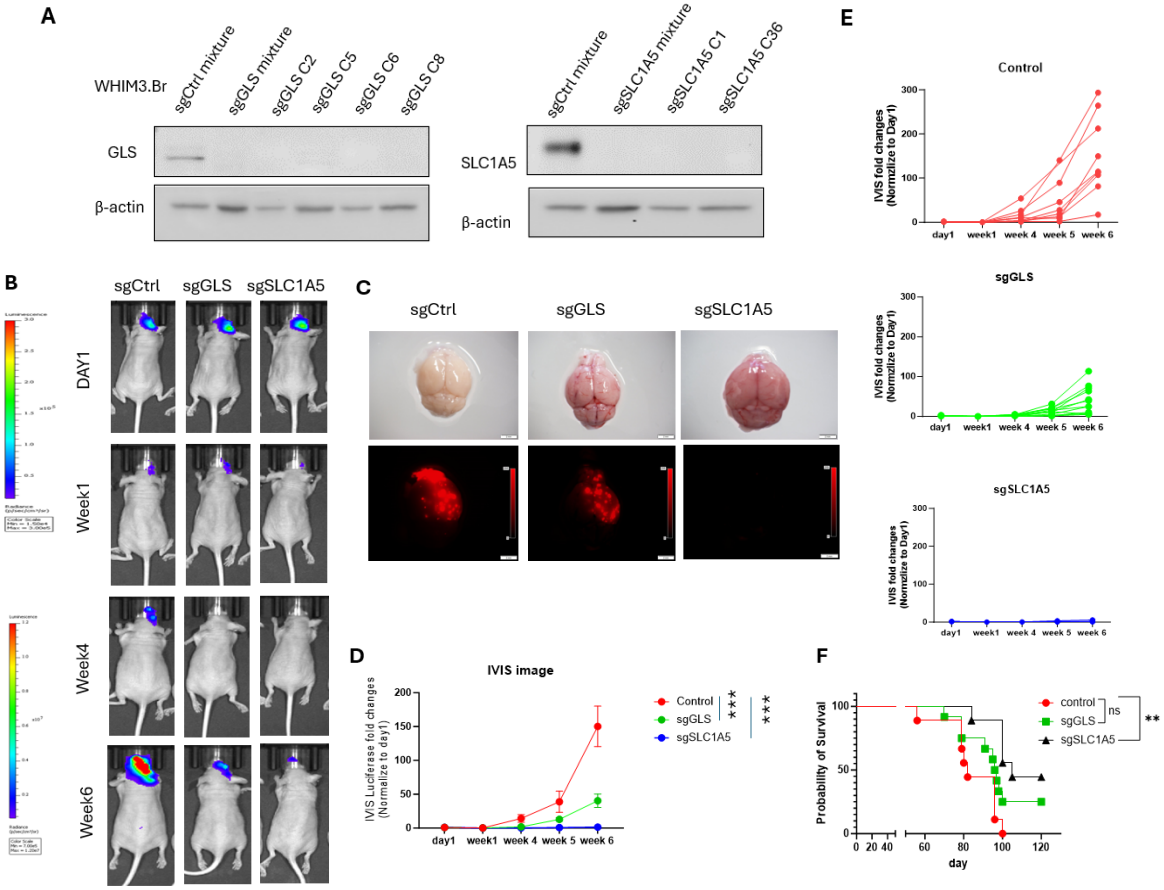

Figure 1: Knocking out GLS or SLC1A5 in WHIM3Br cells significantly blocked BrM. (A). Western blot showing GLS, SLC1A5, β-actin expressions in indicated WHIM3Br sublines or single clones. (B). The representative bioluminescence (BLI) of BrM lesions in the groups of ICA injected with sgCtrl, sgGLS or sgSLC1A5 cells from day 1 post ICA injection to 6 weeks. (C). The representative bright light image and RFP fluorescence image of brains in the mouse ICA injected with sgCtrl, sgGLS or sgSLC1A5 cells at 6 weeks post injection. (D). Quantification of BLI fold change of BrM lesions in three groups during day 1 to 6 weeks after injection. BLI is normalized according to the signal on the first day after injection. Statistics is represented as mean ± s.e.m, t-test, ***, P < 0.001. (E). Quantification of BLI fold change of BrM lesions in each mouse of three groups. BLI is normalized according to the signal on the first day after injection. (F). Kaplan-Meier curves showing overall survival of mice ICA injected with sgCtrl, sgGLS or sgSLC1A5 cells. $^{**}P < 0.01$, log-rank test.

To investigate the effect of SLC1A5 or GLS gain-of-function on BrM outgrowth, we transduced SLC1A5, GLS, or an empty vector plasmid into GFP-labeled MDA-MB-231 brain-seeking cells (231.Br), successfully generating SLC1A5-overexpressing (231Br.SLC1A5.OE), GLS-overexpressing (231Br.GLS.OE), and control vector-transduced (231Br.Vector) cell lines (Figure 2A, 2B).

First, we assessed cell proliferation using the MTT assay. When cultured in DMEM/F12 medium with 10% fetal bovine serum (FBS), all three sublines showed no significant differences in proliferation rates (Figure 2C). However, under nutrient-limited conditions mimicking the brain microenvironment—using basal Eagle's Minimal Essential Medium (BME) supplemented with 5% dialyzed FBS (5% d.FBS) and 500 μM glutamine—231Br. GLS.OE cells exhibited a significantly higher proliferation rate compared to both 231Br.Vector and 231Br.SLC1A5.OE cells (Figure 2D). Next, we examined the invasive capacity of 231Br.GLS- or SLC1A5-OE cells. The results showed that overexpression of either GLS or SLC1A5 did not significantly alter cell invasion ability (Figure 2E). Based on these in vitro findings, we proceeded to investigate the in vivo effect of GLS overexpression on BrM outgrowth.

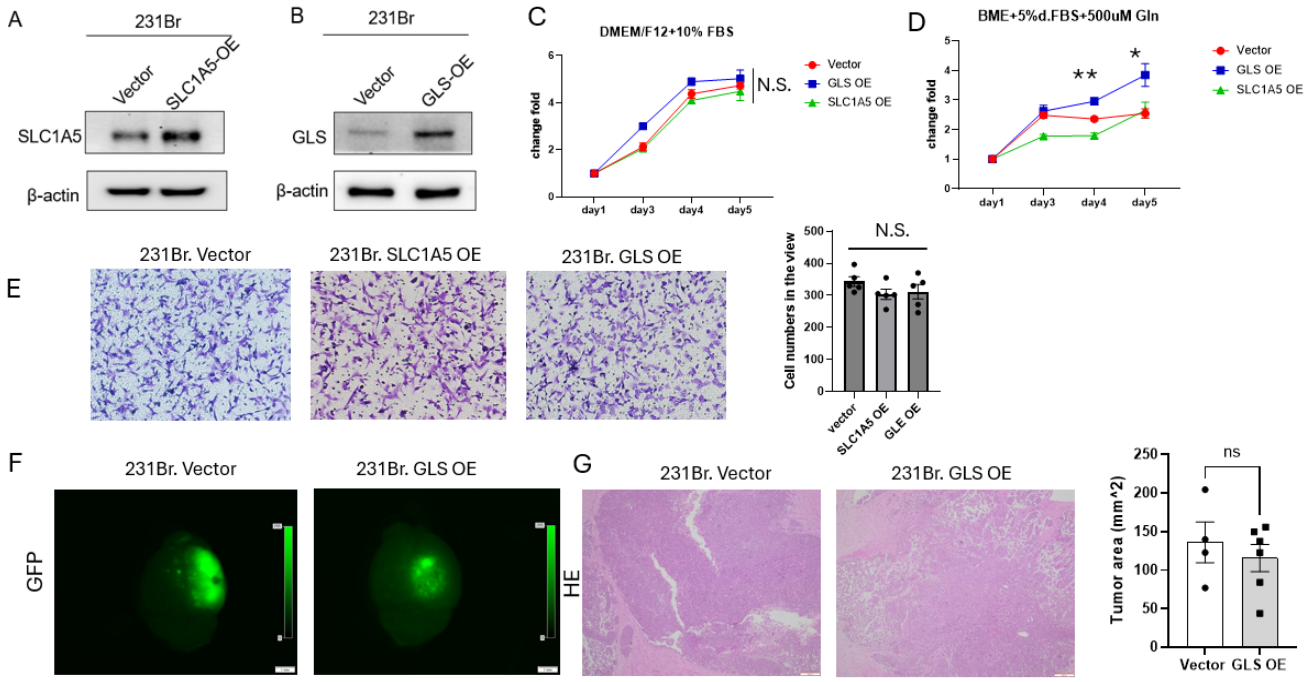

Figure 2. Gain of GLS function in 231Br cells did not promote BrM. (A). Western blot showing SLC1A5 and β-actin expressions in 231Br cells. (B). Western blot showing GLS and β-actin expressions in 231Br cells. (C). MTT assay result showing proliferation of 231Br.Vector, 231Br. GLS OE, and 231Br. SLC1A5 OE cells cultured in DMEM/F12+10% FBS. Data are presented as means ± S.E.M., t-test (two-sided). N.S., not significant. (D) MTT assay result showing proliferation of 231Br.Vector, 231Br. GLS OE, and 231Br. SLC1A5 OE cells cultured in BME+5% d.FBS+500uM Gln. Data are presented as means ± S.E.M., t-test (two-sided). **P < 0.01; * P < 0.05. (E). Representative images and quantification of invading 231Br.Vector, 231Br. GLS OE, and 231Br. SLC1A5 OE cells. Data are presented as means ± S.E.M. t-test (two-sided). (F). The representative GFP images of mouse brain injected with 231Br.Vector, 231Br. GLS OE cells at 5 weeks after ICA injection. (G). The representative H&E-stained images and quantification of BrM area in mouse brains injected with 231Br.Vector, or 231Br. GLS OE cells at 5 weeks after ICA injection. Data are presented as means ± S.E.M., t-test (two-sided). ns, not significant.

We injected 100,000 231Br.Vector or 231Br.GLS.OE cells into the carotid artery of nude mice to evaluate the impact of GLS overexpression on BrM progression. Mice were sacrificed five weeks post-injection, and BrM lesions were assessed using fluorescence imaging and H&E staining. Both GFP fluorescence and histological analysis revealed no significant differences in BrM burden between mice injected with 231Br.Vector cells and those injected with 231Br.GLS.OE cells (Figure 2F, 2G). These findings suggest that GLS overexpression alone is not sufficient to promote BC BrM.

In Aim 1, we proposed to investigate the role of GLS and SLC1A5 loss-of-function in metastatic cell dormancy. In Year 1, we assessed Ki67, a marker of proliferation and non-dormancy, in BrM samples from mice bearing WHIM3Br-induced BrMs treated with CB839 or JHU083—both of which inhibit GLS enzymatic activity. The results showed that treatment with either CB839 or JHU083 did not significantly

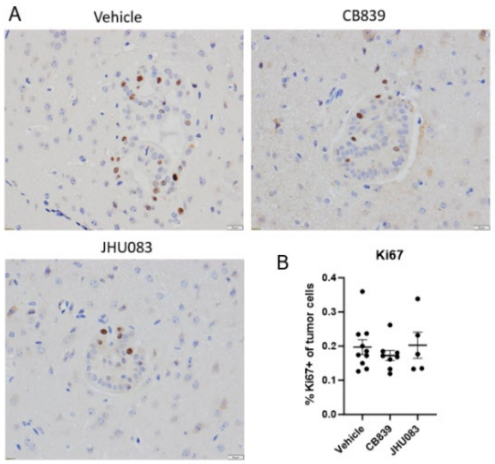

Figure 3. Ki67 IHC staining. (A)-(B) The representative image and quantification of Ki67 IHC staining in Vehicle group, CB839, JHU083 groups. Statistics is represented as mean ± s.e.m, t-test, no significance.

alter Ki67 expression (Figure 3A–B), suggesting that GLS inhibition does not substantially affect metastatic cell dormancy.

In summary, our data clearly demonstrate that GLS and SLC1A5—two key regulators of glutamine metabolism—are critical for the progression of BrM. However, only GLS overexpression is not enough to promote BrM.

Aim 2. Assess the efficacy of pharmacologically blocking glutamine utilization alone, or in combination with immune therapy for BC BrM treatment. *This aim seeks to determine whether targeting glutamine metabolism can serve as an effective and safe therapeutic strategy for BC BrMs, and whether it can enhance the efficacy of immune checkpoint inhibitors (ICIs) and natural killer (NK) cell therapies. In the second year, we will assess the therapeutic potential of JHU083, both as a monotherapy and in combination with ICIs and NK cell therapy, in suppressing BrM progression and improving overall survival in immunocompetent mouse models*

In the first year, we focused on Aim 2.1 to assess the therapeutic potential of inhibiting glutamine metabolism using CB-839 or JHU083 as monotherapies. CB-839, a brain-penetrant and glutaminase (GLS)-specific inhibitor, has demonstrated safety in Phase I clinical trials (NCT02071927, NCT02071888) for hematologic malignancies and is currently being evaluated in combination with chemotherapy for solid tumors, including brain tumors (NCT03528642, NCT04250545, NCT03875313). JHU083 is an orally bioavailable, brain-penetrant prodrug of 6-diazo-5-oxo-L-norleucine (DON), designed to remain inert in circulation to minimize systemic toxicity while releasing an active glutamine antagonist within brain tumors[4]. JHU083 has been shown to inhibit GLS activity and purine biosynthesis[5,6]. Our data demonstrated that both CB-839 and JHU083 effectively suppressed BC BrMs in immunodeficient mouse model, with JHU083 showing particularly promising results that exceeded our expectations. Based on these findings, we have prioritized JHU083 for further investigation, both as a monotherapy and in combination with anti- programmed cell death protein 1 (PD-1) ICI immunotherapy and NK cell therapy, in immunocompetent mouse models of BrM.

Before conducting in vivo experiments, we assessed the effect of DON on NK cell cytotoxicity in vitro. The mouse breast cancer cell line EO771 was labeled with DiO (green fluorescence) and subjected to one of the following treatments for 24 hours: vehicle control, DON (10 μM), co-culture with NK cells at a 1:1 ratio, or co-culture with NK cells cells at a 1:1 ratio in the presence of DON (10 μM). Fluorescence imaging showed that DON alone did not affect tumor cell viability within 24 hours. As expected, NK cells effectively killed EO771 tumor cells, and this cytotoxic effect was further enhanced by DON treatment (Figure 4A). Cell viability was also assessed by flow cytometry, yielding results consistent with the fluorescence images (Figure 4A). A similar experiment was performed using another mouse breast

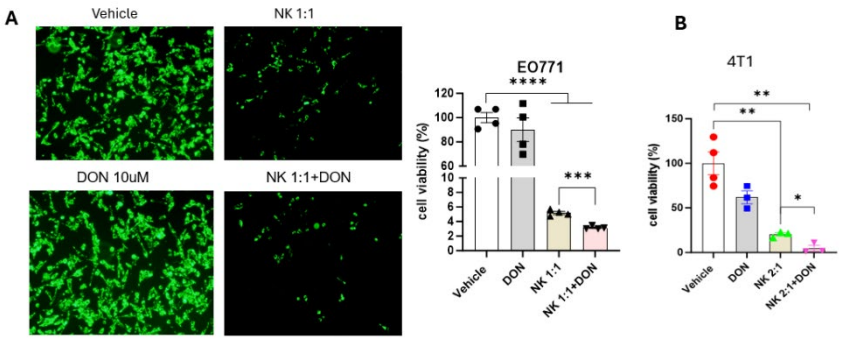

Figure 4: DON treatment further improved human nature killer (NK) cells' cytotoxicity. (A) The representative fluorescent pictures of EO771 cells treated with vehicle, DON, NK cells (ratio to tumor cells 1:1), or NK cells (ratio to tumor cells 1:1) with DON, and the quantification of EO771 viability (%) after vehicle, DON treatment, NK cell coculture or DON combined with NK cell co-culture. (B) The quantification of 4T1 viability (%) after vehicle, DON treatment, NK cell coculture (ratio to tumor cells 2:1), or DON combined with NK cell coculture (ratio to tumor cells 2:1).

cancer cell line, 4T1, which demonstrated comparable results. These findings suggest that DON enhances the anti-tumor activity of NK cells in vitro.

To evaluate the efficacy of JHU083 treatment alone and in combination with immunotherapies or NK cell therapy in an immunocompetent BrM mouse model, we intracranially injected 2,000 EO771 cells into 58 C57BL6 mice and initiated treatment on Day 7 post-injection. The mice were divided into six groups: 1) Control group (n = 10): Treated with vehicle by oral gavage and control IgG via intraperitoneal (i.p.) injection. 2) JHU083 group (n = 9): Treated with JHU083 at 1 mg/kg during the first week and 0.03 mg/kg during the following three weeks via oral gavage, along with control IgG via i.p. injection. 3) NK cell group (n = 9): Received 1 million activated NK cells via intratumoral injection on Days 7 and 14, along with vehicle via oral gavage. 4) Anti–PD-1 group (n = 10): Treated with anti–PD-1 antibody (200 μg/mouse) via i.p. injection every 3 days for a total of five doses, along with vehicle via oral gavage. 5) JHU083 + anti–PD-1 group (n = 10): Received JHU083 as in Group 2 and anti–PD-1 antibody as in Group 4. 6) JHU083 + NK cells group (n = 10): Treated with JHU083 as in Group 2 and NK cells as in Group 3 (Figure 5A). Brain tumor lesions were evaluated by MRI on Day 18 post-injection (Figure 5B). MRI analysis of brain tumor lesions revealed that JHU083 treatment alone significantly inhibited BrM progression (Figure 5B, 5C).

In the anti–PD-1 treatment group, two distinct subpopulations emerged: two mice developed large brain tumors, while the remaining mice exhibited smaller lesions compared to the vehicle group. This suggests possible resistance to anti–PD-1 immunotherapy in a subset of mice. Treatment with NK cells showed a trend toward reduced brain metastasis burden relative to the vehicle group, although the

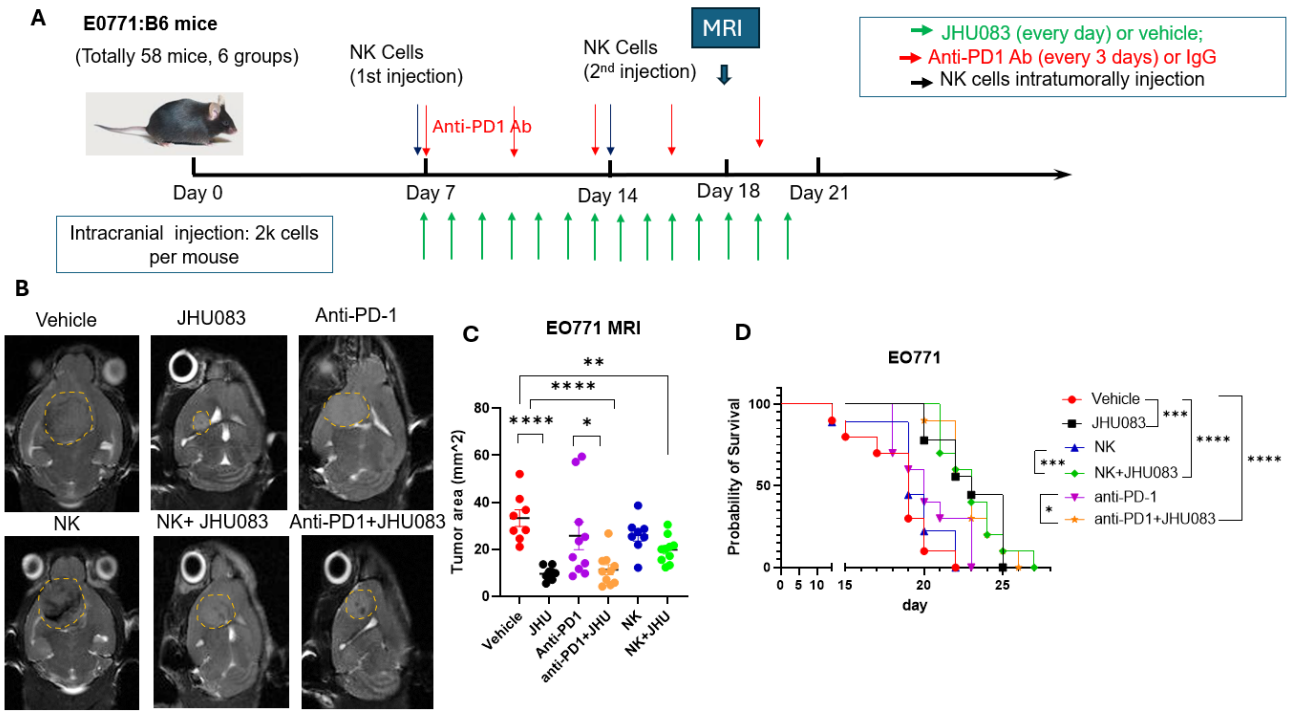

Figure 5: Glutaminase inhibitor JHU083 efficiently inhibited BMs induced by EO771 cells. (A) Schematic representation of BrM mouse model establishment and treatment design. (B) The representative MRI picture of brain tumor lesions in the vehicle, JHU083 treatment, anti-PD1 treatment, NK cell treatment, NK with JHU083 treatment, and anti-PD1 with JHU083 treatment group at day 18 post ICA injection. (C) Quantification of brain tumor lesion area in MRI image in six indicated groups at day 18 post ICA injection. Statistics is represented as mean ± s.e.m, t-test *, $P < 0.05$; **, $P < 0.01$; ***, $P < 0.001$; ****, $P < 0.0001$. (D)). Kaplan-Meier curves showing overall survival of six indicated groups of mice. ***, $P < 0.001$; ****, $P < 0.0001$, log-rank test.

difference was not statistically significant. Combination treatments with JHU083 and either anti–PD-1 antibody or NK cells did not demonstrate additional inhibitory effects beyond that observed with JHU083 monotherapy (Figure 5B–5C).

Survival analysis further supported these findings. Mice treated with JHU083 alone, JHU083 plus anti–PD-1, or JHU083 plus NK cells showed improved survival compared to the other three groups (Figure 5D), consistent with the observed differences in brain metastasis volume among the groups.

We sought to understand why NK cell therapy did not show significant inhibitory effects in this mouse model. Several possible explanations may account for this observation: 1) Limited in vivo persistence and function: Although NK cells isolated from mouse spleens and expanded in vitro with IL-15 exhibited strong cytotoxicity against tumor cells (Figure 4), we were unable to assess their viability and functional activity following intratumoral injection. It is possible that their survival or cytotoxic capacity

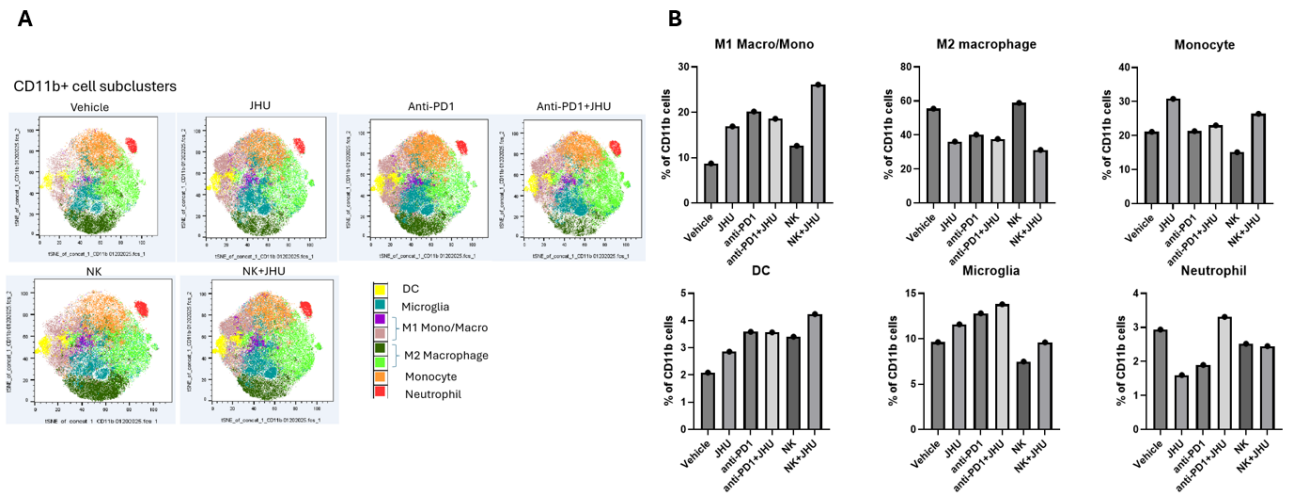

Figure 6: JHU083 treatment increased M1-like macrophage, monocyte, microglia and DC cells, and reduced M2-like macrophage and neutrophils. (A) t-SNE plots based on CyTOF to show the CD11b+ myeloid cell subcultures in the indicated groups. (B) The quantification of CD11b+ myeloid cell subcultures in the indicated groups.

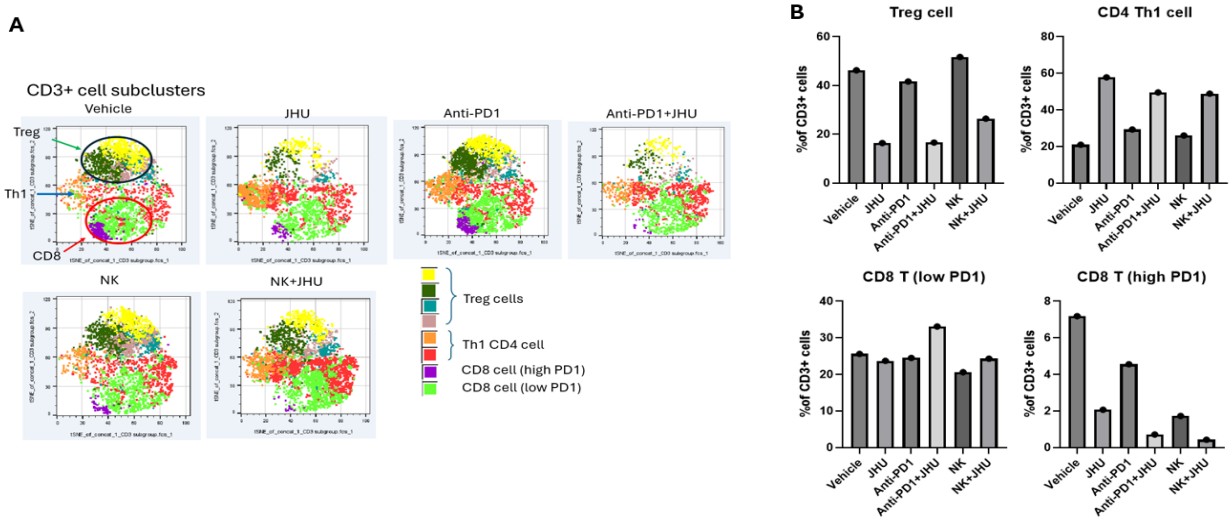

Figure 7: JHU083 treatment increased CD4 Th1 cells, monocyte, and reduced Treg cells and high-PD1 CD8 T cells. (A) t-SNE plots based on CyTOF to show the CD3+ T cell subcultures in the indicated groups. (B) The quantification of CD3+ T cell subcultures in the indicated groups.

was compromised in the tumor microenvironment. 2) Procedure-induced local inflammation: NK cells were administered via intratumoral injection using an implantable guide-screw system, which was used twice. This procedure induced local inflammation, as evidenced by reddish skin around the wound site. Such inflammation may have negatively affected the in vivo functionality of the injected NK cells, potentially impairing their anti-tumor efficacy.

To investigate how treatment alters the brain immune microenvironment, we randomly selected four mouse brains from each group and isolated live CD45$^+$ immune cells for CyTOF analysis. Within the CD11b$^+$ myeloid compartment, six distinct subpopulations were identified: M1-like macrophages, M2-like macrophages, monocytes, neutrophils, microglia, and dendritic cells (DCs) (Figure 6A). M1-like macrophages are pro-inflammatory and associated with anti-tumor immunity, whereas M2-like macrophages are typically anti-inflammatory and support tumor progression[7]. JHU083 monotherapy led to an increased proportion of M1-like macrophages, monocytes, microglia, and DCs, along with a reduction in M2-like macrophages within brain tumor lesions. The combination of JHU083 with either anti–PD-1 antibody or NK cells resulted in a similar pattern of myeloid cell reprogramming as observed with JHU083 alone (Figure 6B). In the CD3$^+$ lymphocyte population, four major subtypes were identified: regulatory T cells (Tregs), CD4$^+$ Th1 cells, CD8$^+$ T cells with high PD-1 expression (potentially exhausted), and CD8$^+$ T cells with low PD-1 expression (Figure 7A). JHU083 treatment increased the proportion of CD4$^+$ Th1 cells while reducing Tregs and PD-1 high CD8$^+$ T cells. These changes suggest a shift toward a more active anti-tumor immune profile. Similar immune remodeling was observed in the JHU083

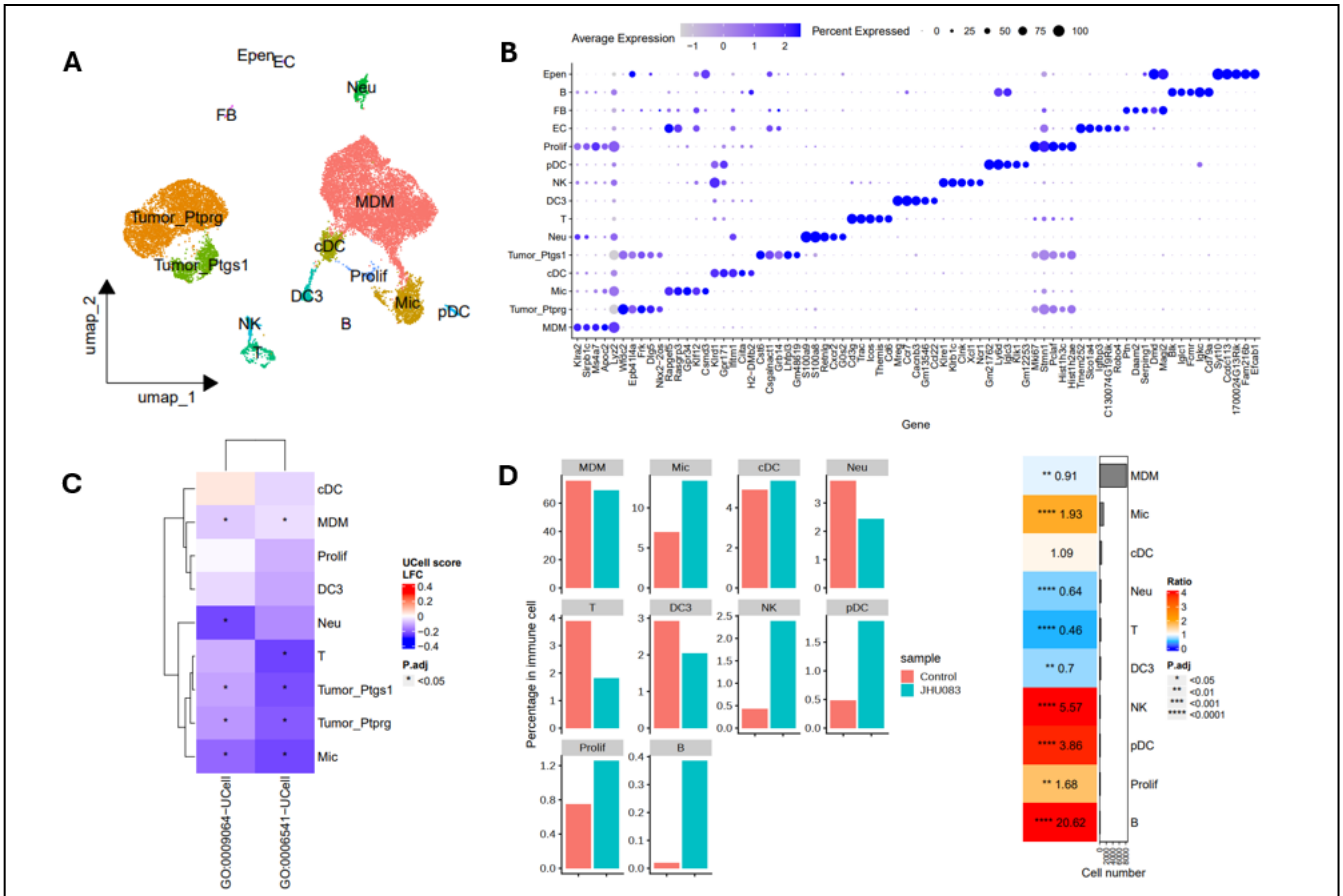

Figure 8: JHU083 treatment changed brain immune microenvironment. (A). Cell types identified in brain metastasis lesions using a UMAP projections of scRNA-seq data. (B) The expression level of cell-type-specific markers. (C) The score of glutamine related pathway (GO:0006541 glutamine metabolic process; GO:0009064 glutamine family amino acid metabolic process) in indicated cell types. (D) The percentage of cell types in Control (vehicle) group and JHU083 groups and the ratio of cell subtypes compared JHU083 group with Control groups with P value.

combined with anti-PD1 or NK cell groups (Figure 7B). Overall, the CyTOF analysis indicates that JHU083 significantly reprograms the brain tumor immune microenvironment toward a pro-inflammatory, anti-tumor state.

Given that JHU083 treatment alone significantly inhibited BrM, we further analyzed tumor and immune cell populations using single-cell RNA sequencing (scRNA-seq). Live cells were isolated from the brains of four mice per group in both the vehicle (control) and JHU083-treated groups and submitted for scRNA-seq analysis. Graph-based Uniform Manifold Approximation and Projection (UMAP) identified 15 major cell types based on the expression of canonical marker genes: two tumor subgroups (Tumor_Ptprg and Tumor_Psgs1), ependymal cells (Epen), B cells, fibroblasts, endothelial cells, proliferating cells, conventional dendritic cells (cDCs), dendritic cells type 3 (DC3), plasmacytoid dendritic cells (pDCs), NK cells, T cells, neutrophils, microglia (Mic), and monocyte-derived macrophages (MDMs) (Figure 8A, 8B). To assess the impact of the glutamine antagonist JHU083, we first analyzed glutamine-related pathways using gene ontology terms: GO:0006541 (glutamine metabolic process) and GO:0009064 (glutamine family amino acid metabolic process). The analysis revealed that both tumor subgroups, macrophages, and microglia showed significantly reduced activity in both glutamine pathways. Neutrophils and T cells exhibited decreased glutamine metabolism in one of the two pathways (Figure 8C). These findings suggest that JHU083 directly targets tumor cells, macrophages, and microglia, and partially affects neutrophils and T cells. In terms of immune cell composition, JHU083 treatment significantly increased the proportions of microglia, NK cells, pDCs, proliferating cells, and B cells, while reducing the frequencies of macrophages, neutrophils, T cells, and DC3s (Figure 8D). These changes are consistent with those observed in the CyTOF data, further supporting the conclusion that JHU083 reprograms the brain immune microenvironment toward an anti-tumor state.

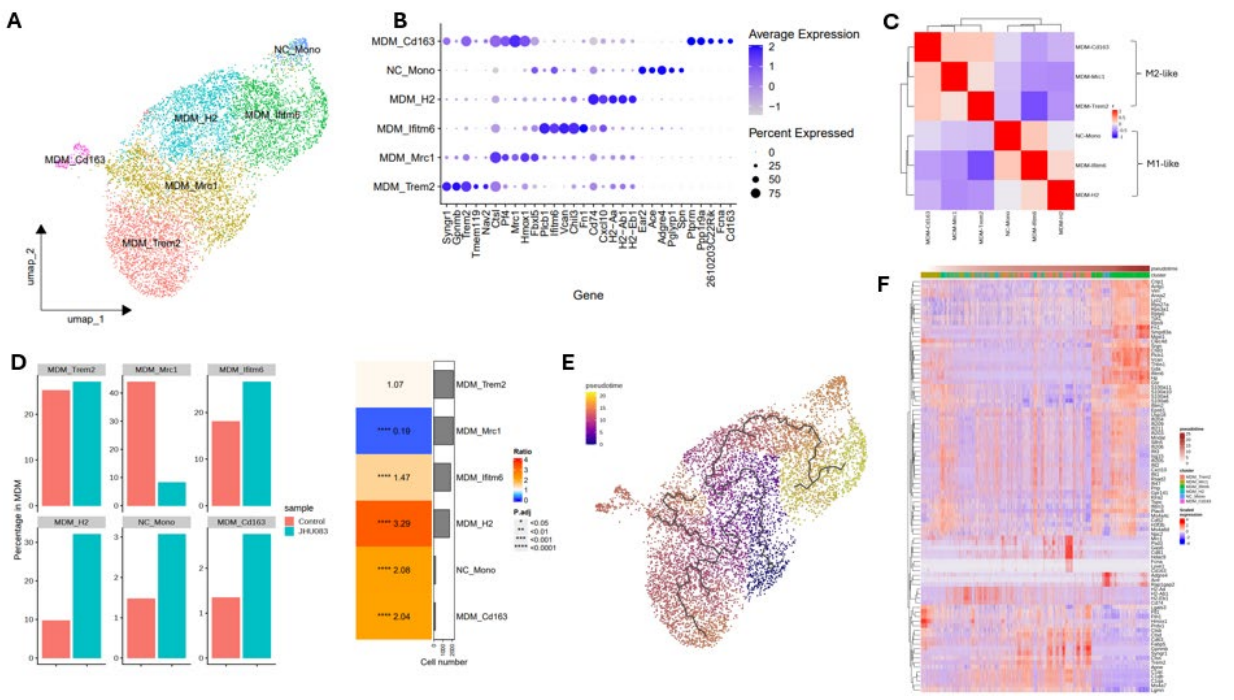

Figure 9: JHU083 treatment increased M1-like macrophage and induced macrophage differentiation to MDM_ifitm6 and MDM_H2 subtypes. (A). Macrophage subtypes identified in brain metastasis lesions using a UMAP projections of scRNA-seq data. (B). The expression level of cell-type-specific markers. (C). The correlation heatmap of MDM six subgroups. (D). The percentage of cell types in Control (vehicle) group and JHU083 groups and the ratio of cell subtypes compared JHU083 group with Control groups with P value. (E). Velocity pseudotime of MDM six subgroups using Monocle 3. (F). Heatmaps showing the expression patterns of significant genes (rows) by cells (columns) ordered by pseudotime.

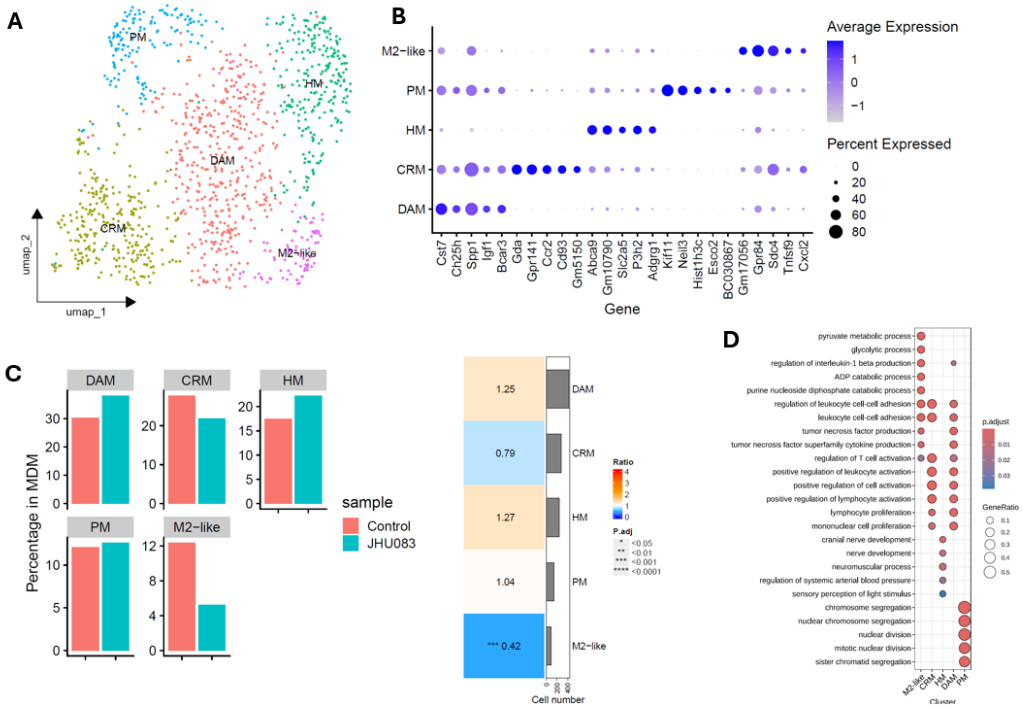

Figure 10: JHU083 treatment increased DAM, HM and reduced CRM and M2-like microglia. (A) Microglia subtypes identified in BrM lesions using a UMAP projections of scRNA-seq data. (B). The expression level of cell-type-specific markers. (C). The percentage of cell types in Control (vehicle) group and JHU083 groups and the ratio of cell subtypes comparing JHU083 group with Control groups with P value. (D). The enriched function pathway of microglia five subgroups.

We further analyzed macrophages (MDMs), the dominant immune cell population within brain tumor lesions. UMAP clustering revealed six distinct MDM subpopulations: MDM_CD163, MDM_Mir1, MDM_Trem2, MDM_Mono, MDM_ifitm6, and MDM_H2 (Figure 9A, 9B). Correlation analysis indicated that MDM_CD163, MDM_Mir1, and MDM_Trem2 are more closely related and exhibit features associated with M2-like, immunosuppressive phenotypes. In contrast, MDM_ifitm6, MDM_H2, and MDM_Mono are more closely related to each other and display characteristics consistent with M1-like, pro-inflammatory phenotypes (Figure 9C). Compared to the control (vehicle) group, JHU083 treatment reduced the proportion of MDM_Mrc1 (an M2-like population) and increased MDM_ifitm6, MDM_H2, MDM_CD163, and MDM_Mono populations (Figure 9D). MDM_Mrc1 was the largest macrophage subpopulation in the control group and is associated with anti-inflammatory, pro-tumor function. Its reduction following treatment suggests a shift toward a more immunostimulatory environment. Notably, JHU083 increased the abundance of MDM_ifitm6, MDM_H2, and MDM_Mono cells, which are linked to a pro-inflammatory response. To better understand the developmental dynamics of these macrophage subsets, we performed pseudotime trajectory analysis using Monocle 3. This analysis indicated that MDM_ifitm6 and MDM_H2 represent more differentiated states of macrophages and are enriched for interferon (IFN) response gene signatures (Figure 9E, 9F), suggesting that JHU083 promotes macrophage maturation toward an IFN-responsive, and anti-tumor phenotype.

In addition to macrophages, microglia (Mic) represented a significantly increased immune population following JHU083 treatment. UMAP analysis revealed five distinct microglial subpopulations: disease-associated microglia (DAM), cytokine-responsive microglia (CRM), homeostatic microglia (HM), proliferating microglia (PM), and M2-like microglia (Figure 10A, 10B). JHU083 treatment notably increased the DAM, HM, and PM subpopulations, while significantly reducing M2-like microglia (Figure 10C). Among these, DAM constituted the dominant microglial subpopulation. Functional enrichment analysis indicated that DAM cells are primarily involved in tumor necrosis factor (TNF) signaling, as well

as the regulation of leukocyte and T cell activation (Figure 10D). These findings suggest that JHU083 treatment not only increased the overall number of microglia (Figure 8D) but also shifted their functional phenotype toward a DAM-like state. This phenotype is associated with enhanced TNF pathway activation and the potential to promote broader immune cell activation within the brain tumor microenvironment.

Although CD3$^+$ T cell infiltration in the EO771-BrM model was limited (Figure 8A), we further analyzed the T cell subpopulations present within the brain. Six distinct T cell clusters were identified: CD8_T cells, proliferating T cells (Prolif_T), CD4$^+$ helper T cells (CD4_Th), regulatory T cells (CD4_Treg), Runx1-expressing T cells (Runx1_T), and CD200-expressing T cells (CD200_T) (Figure 11A, 11B). Correlation analysis revealed that CD200_T cells were closely related to CD4_Treg cells, while Runx1_T cells showed similarity to CD4_Th cells (Figure 11C). JHU083 treatment led to a reduction in immunosuppressive CD4_Treg and CD200_T cells, while increasing the proportion of CD4_Th cells

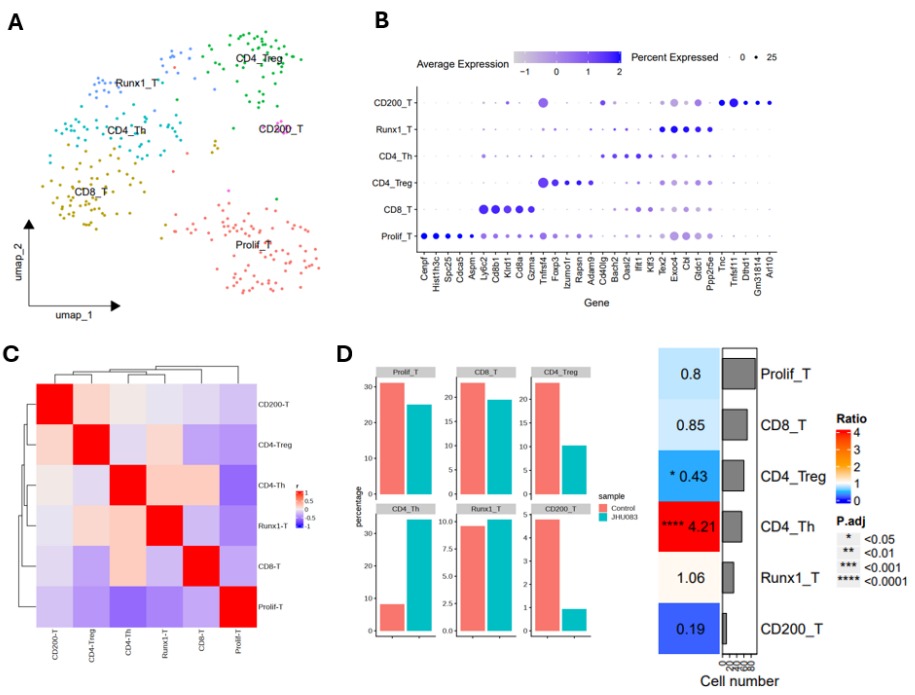

Figure 11. JHU083 treatment increased Th1 CD4 and reduced Treg cells. (A) T cell subtypes identified in BrM lesions using a UMAP projections of scRNA-seq data. (B). The expression level of cell-type-specific markers. (C). The correlation heatmap of T cell six subgroups (D). The percentage of cell types in Control (vehicle) group and JHU083 groups and the ratio of cell subtypes compared JHU083 group with control groups with P value.

(Figure 11D). These changes in T cell composition suggest a shift toward a more pro-inflammatory, anti-tumor T cell response. The scRNA-seq data align with CyTOF findings, both indicating that JHU083 promotes CD4$^+$ Th1-like T cell-mediated anti-tumor immunity within the brain microenvironment.

Since myeloid cells were enriched in our BrM, we further analysis the function of infiltrated myeloid cells such as microglia, macrophage and cDCs. The common enriched pathways in myeloid cells are cellular response to IFN-beta and inflammasome-mediated pathway (Figure 12). pDCs are recognized as the most potent producers of IFN-alpha[8], and cDC and macrophage can produce IFN-beta through the cGAS-STING pathway[9], which is activated by the recognition of cytosolic DNA. This DNA can originate from tumor cells, especially under JHU083 treatment. JHU083 is reported to increase ROS in tumor cells[10], which might damage mitochondria and nuclear DNA, leading to DNA leakage into the cytosol, resulting the cGAS-STING pathway activation in cDC and macrophages. At the same time, tumor cells themselves might also activate the cGAS-STING pathway and release IFN-beta[11]. In the future, we

will further explore the mechanism of how JHU083 activates IFN-beta pathway in myeloid cells and tumor cells.

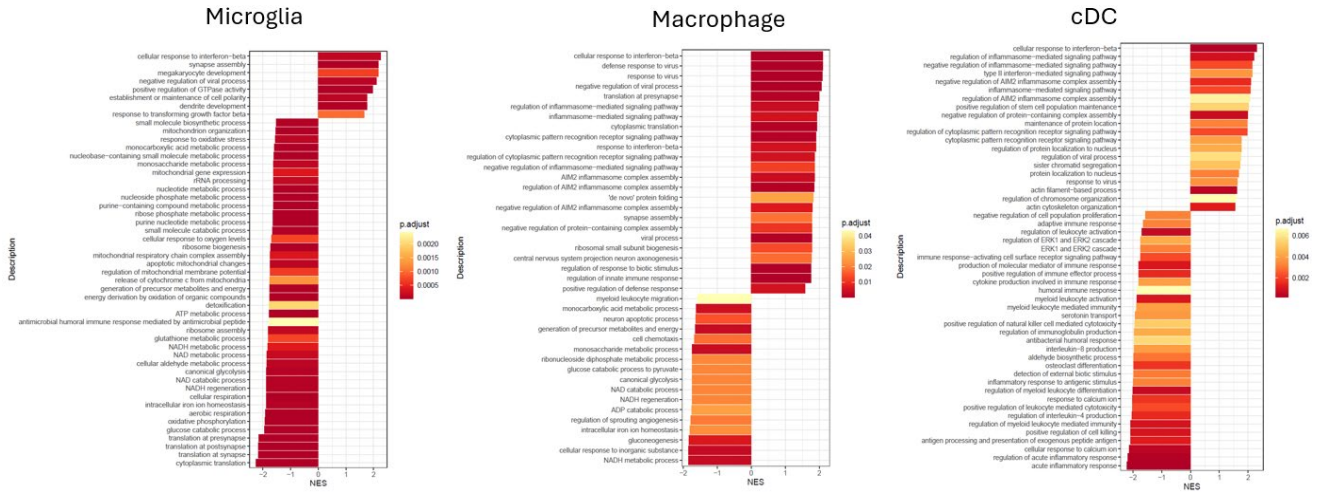

Figure 12. GSEA analysis to show the top upregulated and down regulated pathways in microglia, macrophages and cDC cells comparing JHU083 treatment verse control group.

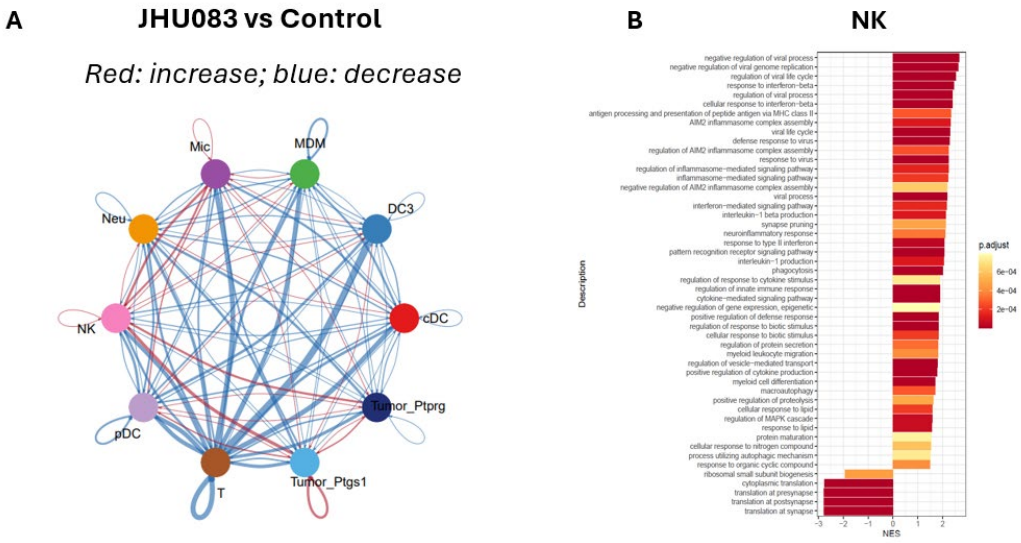

Figure 13. JHU083 treatment increase the cell-cell contact between microglia to NK cells, and NK cells to tumor cells. (A) Cell-cell communication networks inferred from expression of ligand-receptor pairs. showing the differential number of ligand-receptor interactions between JHU083 treatment and Control groups. (B) GSEA analysis to show the top upregulated and down regulated pathway in NK cells comparing JHU083 treatment verse Control group.

Finally, we analyzed cell–cell communication using CellChat. The results showed that JHU083 treatment enhanced the interaction between microglia and NK cells, as well as between NK cells and two tumor cell subpopulations (Figure 13A). Gene set enrichment analysis (GSEA) revealed that NK cells from the JHU083-treated group exhibited enrichment in IFN-β response and inflammasome-mediated pathways, along with increased activity in cytokine-mediated signaling pathways, compared to the control group (Figure 13B).These findings support a novel hypothesis: JHU083 activates microglial cells, which may in turn recruit and stimulate NK cells, enhancing their cytotoxic function against tumor cells. The underlying molecular mechanisms of this interaction will be further investigated.

In summary, we successfully completed all proposed aims and generated compelling evidence that glutamine blockade with JHU083 suppresses BC BrM by simultaneously inhibiting tumor cell mitochondrial respiration and glutamine metabolism, and by reshaping the immune microenvironment to favor anti-tumor responses, particularly by shifting macrophages and microglia toward pro-inflammatory phenotypes, increasing $CD4^+$ Th1-like cells, and enhanced communication between microglia, NK cells, and tumor cells, along with increased IFN-β signaling and cytokine responses in NK cells.

Lay Description of Important Outcomes:

- Summary of our findings
    - **Genetic Targeting of Glutamine Metabolism Inhibits Brain Metastasis**: Genetic knockout of *GLS* (glutaminase) or *SLC1A5* (a glutamine transporter) in WHIM3Br breast cancer cells significantly inhibited BrM formation, highlighting the essential role of glutamine metabolism in supporting BrM outgrowth. However, overexpression of *GLS* did not further promote BrM, suggesting a threshold effect or saturation of glutamine metabolic dependency.
    - **Brain Penetration and Target Engagement:** Both the glutamine antagonist JHU083 and the glutaminase inhibitor CB839 can cross the blood–brain barrier and effectively inhibit GLS activity within BrM lesions and the surrounding brain tissue.
    - **Therapeutic Efficacy in PDX Model:** In the WHIM3.Br PDX TBC model, both JHU083 and CB839 significantly impeded BC BrM progression without observable toxicity. JHU083 demonstrated superior efficacy compared to CB839 in reducing tumor burden and delaying disease progression.
    - **Immunocompetent Mouse Model Findings**: In the EO771-C57BL/6 immunocompetent BrM model, JHU083 monotherapy significantly suppressed BC BrM outgrowth. However, JHU083 did not show a synergistic effect when combined with ICI, suggesting that its primary benefit in this model is as a standalone agent.
    - **Modulation of the BrM Immune Microenvironment**: JHU083 treatment led to 1) reduction in immunosuppressive cell types: M2-like macrophages, regulatory T cells Tregs, and neutrophils. 2) Increase in pro-inflammatory and anti-tumor immune cells: M1-like macrophages, microglia, $CD4^+$ Th1 cells, pDCs, and NK cells. JHU083 treatment shifted macrophages and microglia toward pro-inflammatory phenotypes, increasing IFN-responsive subpopulations and enhanced CD4 Th1 cell and NK cells' anti-tumor immunity.
    - **Enhanced Innate Immune Activation**: JHU083 treatment induced increased IFN-β signaling in infiltrating myeloid cells. JHU083 enhanced the interaction between microglia and NK cells, as well as between NK cells and tumor cells—potentially promoting NK cell recruitment and cytotoxic activation within the BrM microenvironment.

The impact this METAvivor grant has had on the following:

Research impact:

- These studies provide novel and in-depth insights into the critical role of glutamine metabolism in the progression of BC BrM, highlighting its potential as a therapeutic target.
- We demonstrate an intimate and dynamic interplay between tumor cell metabolism and immune cell metabolism within the BrM microenvironment, offering a metabolic framework for understanding immune suppression and resistance in BrM.

- Our work is the first to report that JHU083 treatment promotes infiltration of both microglia and NK cells and enhances their interaction—contributing to a more robust anti-tumor immune response in the brain.
- We show that JHU083 induces broad activation of the interferon-beta (IFN-β) pathway in myeloid cells and microglia, a shift that may drive increased cytotoxicity of both NK cells and $CD4^+$ Th1 cells against tumor cells.

Funding impact:

The preliminary data will help us to submit a strong R01 grant applications to NIH or a Breakthrough Award to the Department of Defense Breast Cancer Research Program in collaboration with our clinical collaborator, Dr. Nuhad Ibrahim, a breast medical oncologist specialized in treating brain metastasis at MD Anderson Cancer Center.

Publications:

We attended AACR annual meeting 2024 and made a poster to introduce our findings, having a good discussion with other attendees. After we complete the added aim, we will submit our manuscript to a high impact peer-reviewed journal.

Impact on patient - treatment, outcomes, etc.

Our findings suggest that the glutamine antagonist JHU083 is a promising therapeutic option for patients at high risk of developing brain metastases.

References

1 Yoo, H. C. *et al.* A Variant of SLC1A5 Is a Mitochondrial Glutamine Transporter for Metabolic Reprogramming in Cancer Cells. *Cell Metab* **31**, 267-283 e212 (2020). https://doi.org/10.1016/j.cmet.2019.11.020

2 Yoo, H. C., Yu, Y. C., Sung, Y. & Han, J. M. Glutamine reliance in cell metabolism. *Exp Mol Med* **52**, 1496-1516 (2020). https://doi.org/10.1038/s12276-020-00504-8

3 Ma, C. X. *et al.* Targeting Chk1 in p53-deficient triple-negative breast cancer is therapeutically beneficial in human-in-mouse tumor models. *J Clin Invest* **122**, 1541-1552 (2012). https://doi.org/10.1172/JCI58765

4 Hanaford, A. R. *et al.* Orally bioavailable glutamine antagonist prodrug JHU-083 penetrates mouse brain and suppresses the growth of MYC-driven medulloblastoma. *Transl Oncol* **12**, 1314-1322 (2019). https://doi.org/10.1016/j.tranon.2019.05.013

5 Alden, R. S., Kamran, M. Z., Bashjawish, B. A. & Simone, B. A. Glutamine metabolism and radiosensitivity: Beyond the Warburg effect. *Front Oncol* **12**, 1070514 (2022). https://doi.org/10.3389/fonc.2022.1070514

6 Yamashita, A. S. *et al.* The glutamine antagonist prodrug JHU-083 slows malignant glioma growth and disrupts mTOR signaling. *Neurooncol Adv* **3**, vdaa149 (2021). https://doi.org/10.1093/noajnl/vdaa149

7 Gao, J., Liang, Y. & Wang, L. Shaping Polarization Of Tumor-Associated Macrophages In Cancer Immunotherapy. *Front Immunol* **13**, 888713 (2022). https://doi.org/10.3389/fimmu.2022.888713

8 Yu, X. *et al.* Cross-Regulation of Two Type I Interferon Signaling Pathways in Plasmacytoid Dendritic Cells Controls Anti-malaria Immunity and Host Mortality. *Immunity* **45**, 1093-1107 (2016). https://doi.org/10.1016/j.immuni.2016.10.001

9 Gan, Y. *et al.* The cGAS/STING Pathway: A Novel Target for Cancer Therapy. *Front Immunol* **12**, 795401 (2021). https://doi.org/10.3389/fimmu.2021.795401

10 Oh, M. H. *et al.* Targeting glutamine metabolism enhances tumor-specific immunity by modulating suppressive myeloid cells. *J Clin Invest* **130**, 3865-3884 (2020). https://doi.org/10.1172/JCI131859

11 Li, T. & Chen, Z. J. The cGAS-cGAMP-STING pathway connects DNA damage to inflammation, senescence, and cancer. *J Exp Med* **215**, 1287-1299 (2018). https://doi.org/10.1084/jem.20180139